Automatic detection and characterization of the ML on polarimetric RHI scans

Daniel Wolfensberger[1] and Alexis Berne[2]

[1]*Ecole polytechnique fédérale de Lausanne, 1015 Lausanne, Switzerand*
[2]*Ecole polytechnique fédérale de Lausanne, 1015 Lausanne, Switzerand*
(Dated: 20 July 2014)


Daniel Wolfensberger

1. Introduction

The melting layer (ML) is an important feature of precipitation, frequently occurring during stratiform rainfall. It is associated with the melting of snowflakes/ice crystals below the freezing level. It can be seen on meteorological radar RHIs as a thin nearly horizontal layer with a high reflectivity factor and low values of ρ_{hv} (copolar correlation coefficient). The high reflectivity is due to the fact that ice crystals with liquid water at their surface behave as huge water drops in terms of reflectivity, which depends on the sixth power of the drop diameter. The height of the ML gives an indication of the maximal height of the stratiform rain and the altitude of the $0°\mathrm{C}$ isotherm.

The characteristic layer of high reflectivity caused by the ML is often refered to as a bright band. The bright band can bias the estimation of the rain intensity and as such its automatic detection has always been an area of interest for radar meterorologists. However, horizontal reflectivity is often not sufficient to detect the ML as small rainfall cells originating from the melting layer can have a very strong reflectivity too. In addition, the bright-band in Z_h is generally thicker than the melting layer and algorithms solely based on Z_h tend to be overestimating and unreliable.

Fortunately, the ML can be easily identified on polarization radars because it is characterized by a very distinct signature in ρ_{hv} (Figure 1. This polarimetric variable is dependent on the heterogeneity in shape of the hydrometeors. In stratiform rain it is generally high (≥ 0.95) due to the high homogeneity of rain droplets (Matrosov et al., 2007). In the ML, where a mixture of rain and snow occurs it is distinctly smaller (0.7–0.95). In snow the copolar correlation coefficient is around 0.9. In addition, the $0°\mathbb{C}$ isotherm is also characterized by a sharp increase in Z_{dr} due to transition between solid phase where Z_{dr} is usually small (Doviak and Zrnić (2006), p.257) to liquid phase where it is higher. The ML generally appears larger on Z_h than on Z_{dr} and ρ_{hv}. Typically the maximum in Z_h will be at a higher altitude than the minimum in ρ_{hv} and maximum in Z_{dr}. This is due to the fact that Z_h is maximal when the ice crystal start to melt, i.e. when they are still large but coated with a very thin layer of liquid water, ρ_{hv} however is minimal when the mixture between ice crystals and drops is the most heterogeneous. This happens at a lower altitude, when sufficient melting has already occcured.

Considering the great importance of the ML in stratiform rain, our aim is to gather more information about its statistics in terms of polarimetric signature and geometrical shape. To achiveve this goal, we took advantage of the additional information provided by dual-polarimetry and developped a new algorithm for melting layer detection on polarimetric RHI scans based on the detection of strong gradients. We then used this algorithm to characterize the ML using a large dataset of radar scans from different seasons and climatic regions (South of France, Great Plains, Swiss Alps).

2. Main Matter

2.1. Method

2.1.1. Algorithm

Instead of simply adapting an existing algorithm from PPI, we decided to design a new algorithm that works directly in RHI by taking advantage of the fact that gradients in ρ_{hv} and Z_h are usually stronger and better defined in vertical scans.

Our algorithm is based on a slightly different method than the one proposed by (Giangrande et al., 2007). We relied on the presence of sharp edges in the polarimetric variables, especially in ρ_{hv} and proposed an automatic detection routine based on detection of gradient maximas. The algorithm works in the following way:

1. The copolar correlation coefficient ρ_{hv} and the horizontal reflectivity Z_h variables are first projected from polar to Cartesian coordinates.
2. Measurements at very low elevation angles ($0 - 1°$) are removed in order to avoid possible interference from ground clutter.
3. Both variables are then normalized in the range $[0, 60]$ dB $\rightarrow [0, 1]$ for Z_h and $[0.75, 1]$ dB $\rightarrow [0, 1]$ for ρ_{hv}, in order to give a weight of similar magnitude to both variables and to avoid detection of a ML in very weak stratiform situations.

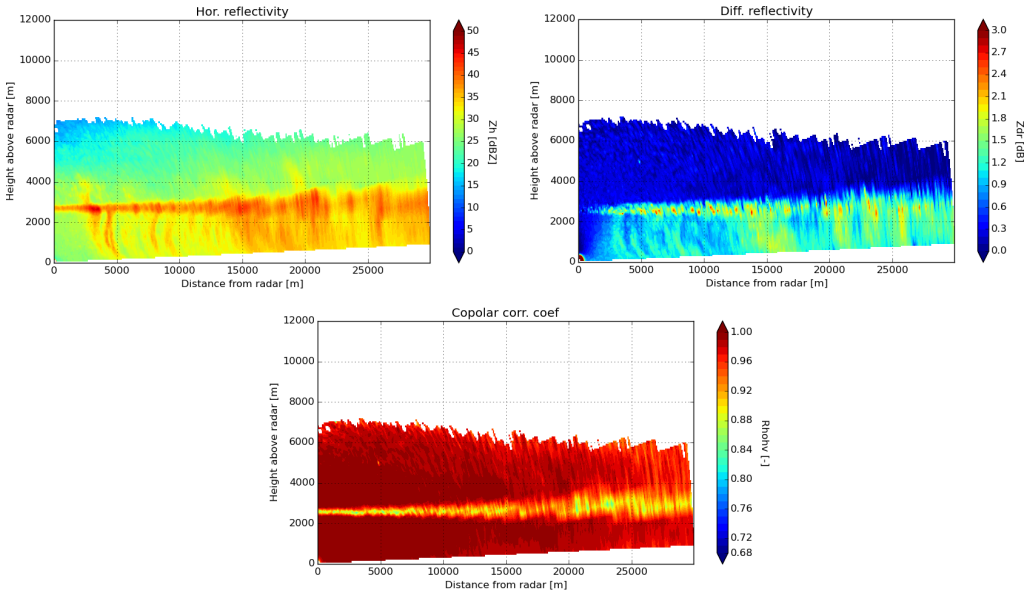

Figure 1: Exemple of the melting-layer signature in Z_h, Z_{dr} and ρ_{hv} in a typical stratiform rain situation in the south of France (29.09.2012 12:24) . The melting-layer is characterized by the combination of a layer of small ρ_{hv} values, a transition from high to low Z_{dr} and the presence of high values in Z_h.

4. After a median filtering of both variables with a moving window of size 250×250 m^2, the normalized variables are combined into a single image:

$$\text{IM}_{\text{comb}} = Z_h \cdot (1 - \rho_{\text{hv}})$$

5. The gradient of the combined image in the vertical direction.

6. The image is scanned column by column (i.e. a vertical cut). The algorithm searches for negative and positive peaks in the 1D gradient signal at each column that exceed a certain threshold $A_{\text{grad, min}}$ (fixed at 0.01). If we consider the positive axis to start from the ground, positive peaks in the gradient correspond to the lower edge of the ML and negative peaks to the upper edge. If both an upper and a lower edge with sufficient intensity are detected, all pixels in between are considered as belonging to the ML. If more than two pixels exceed the threshold, the pair with the strongest gradient difference is retained. An additional check is done on the values of ρ_{hv}: if between the two detected edges, there is no pixel lower than 0.95 OR any pixel higher than 0.6, the edges are considered as suspicious and removed. The first condition comes from the fact that the ML is characterized by low values of ρ_{hv} and the non-detection of any low value is very unlikely. The second conditions comes from the fact that values below 0.6 generally indicate the presence of ground clutter or other non-meteorological echoes (biological scatterers or planes), as they are too low for precipitation.

7. The algorithm works in two consecutive steps: the method described above is first done without any additional integrity check, which may lead on some occasions to pixels being misclassified due to the presence of strong edges caused by the remaining ground clutter or by mistaking convective cells for the ML.The median height of the upper boundary of the ML ($M_{ML,bot}$) and the median height of the lower boundary of the ML ($M_{ML,top}$) are computed at the end of this preliminary step.

8. In the second step, the algorithm is run again but this time after cutting the gradient image above $1.3 \cdot Med_{ML,top}$ and below $0.7 \cdot Med_{ML,bot}$. The hard threshold on gradient intensity has still to be exceeded.

In a last step, small holes (less than 250 m which corresponds to the size of the median filter) are interpolated by piecewise continuous spline interpolation.

2.1.2. Validation

The first parameter of importance is the threshold on the minimal value of the gradient for an edge to be considered. The value of 0.01 was chosen by visual inspection as it was found out that this value is very rarely obtained in situations without ML. It serves as a way to avoid considering edges of too low intensity. It was observed that this contraint does not negatively affect the detection even for relatively weak ML situations.

The second parameter is the constraint on the relative height of the bottom and the top of the ML. In the algorithm it is assumed that the bottom of the ML doesn't fluctuate below 0.7 of the median bottom height and the top above 1.3 of the median top height. To test the validity of this hypothesis, the top and bottom relative heights of the ML were computed for

all time steps of the whole HyMeX campaign for a maximal distance from the radar going up to 20 kilometers, which is the maximal range used in this work. It was shown that for a distance up to 20 kilometers, this assumption can be considered as valid and is a reasonable way to limit the interference of ground-clutter, embedded convective cells or other perturbating echoes (birds, planes,...). For higher distances, this may not be true due to the effect of beam-broadening leading to an increase in the apparent thickness of the ML.

At last, the size limit for interpolation of holes (250 m) was confirmed by inspection of the distribution of hole sizes. It was observed that 75% of all holes were smaller than 250 m and since this value is still reasonably small compared to the usual length of the ML (15-25 km) it should not affect the overall estimation of the ML.

2.2. Results

Some examples of automatic detection of the ML are shown in Figure 2. It is difficult to assess directly the performance of the algorithm as no references such as atmospheric soundings or altitude of the 0°C isotherm are available. However, by considering the transition in ρ_{hv} as the main indicator of the presence of the ML, it can be seen that in most cases the algorithm accurately bounds the position of the ML. The algorithm may however not be very robust in strong convective cells, which are characterized by values in ρ_{hv} similar to the ML. It also seems that the algorithm slightly underestimates the width of the ML, as in some cases very low values of ρ_{hv} incompatible with rain can be found outside the detected ML boundaries.

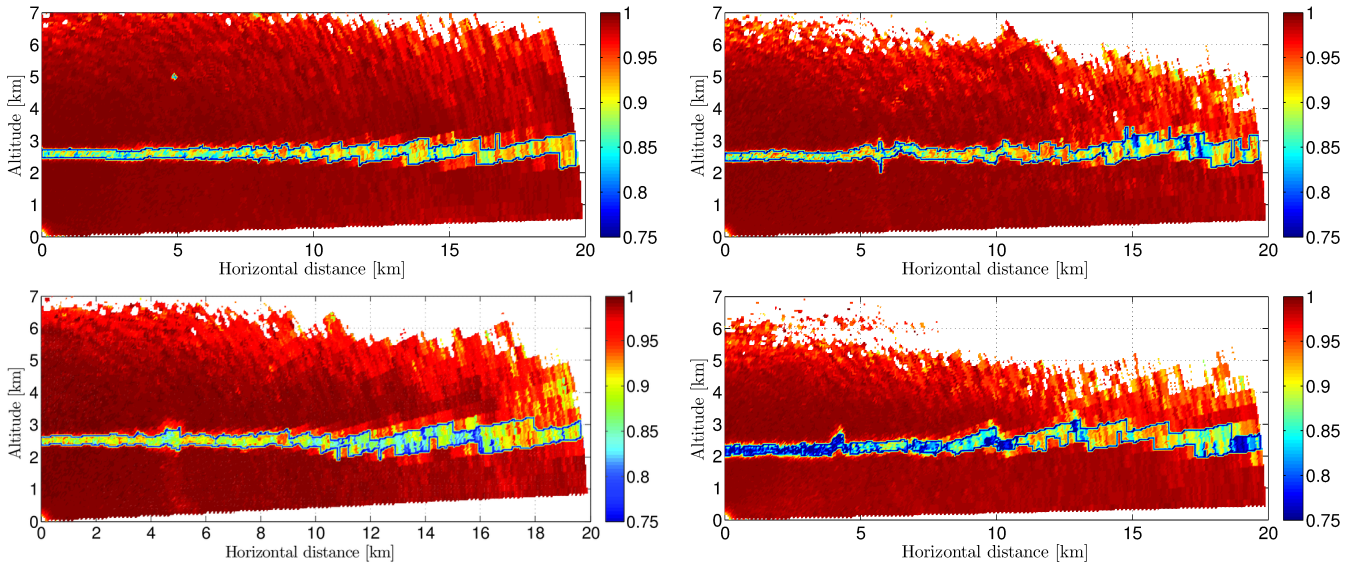

Figure 2: Some examples of ML detection with the associated ρ_{hv} field, the detected ML is shown with a blue contour and white pixels correspond to missing values (low signal/noise ratio or low elevations). We can see that the detected ML contours correspond very well to a sharp transition to smaller values of ρ_{hv} , which is the kind of structures the algorithm is looking for.

The algorithm was used to compute various statistics on a large dataset (more than 10'000 time steps) of vertical radar scans (RHI) obtained during several radar campaigns in different climatic regions and at different seasons, namely in Ardèche (France), in the Great Plains (USA) and in Davos (Swiss Alps). In order to limit the effect of beam broadening which causes a loss of resolution at increasing distances from the radar, only the first 5 kilometers from the radar were considered. No interpolation of the holes in the detected ML was done, in order to avoid introducing artifacts in the characterization. Additionally, Z_h and Z_{dr} were corrected for attenuation in the liquid phase (below the detected ML) using the ZPHI algorithm (Testud et al., 2000). We assumed that attenuation inside the solid phase (in ice clouds above the ML) is probably much smaller and could be neglected (Doviak and Zrnić (2006), p.43).

The distributions of the radar variables Z_h, Z_{dr}, K_{dp}, ρ_{hv} and S_w were computed within the ML, above the ML (solid phase) and below the ML (liquid phase). In addition, six variables linked to the geometry of the ML were computed (Table 1).

$\mathrm{ML}_{\mathrm{Bot},fluct}$	Relative fluctuations of the lower boundary of the ML in [m]. For each scan, the altitude of the bottom of the ML at elevation $90°$ (horizontal distance zero from the radar) is used as the reference height: $$\mathrm{ML}_{\mathrm{Bot},fluct}(x) = \mathrm{ML}_{\mathrm{Bot}}(x) - \mathrm{ML}_{\mathrm{Bot}}(0)$$
$\mathrm{ML}_{\mathrm{Top},fluct}$	Relative fluctuations of the upper boundary of the ML in [m]. For each scan, the altitude of the top of the ML at elevation $90°$ is used as the reference height.
$\mathrm{ML}_{\mathrm{Thickness}}$	Thickness of the ML in meters.
$\gamma_{\mathrm{Bot},fluct}$	Variogram of the relative fluctuations of the lower boundary of the ML. To exclude a potential linear drift in the fluctuations with the horizontal distance, the variogram was calculated on the *residuals* of a linear regression of fluctuations vs distance.
$\gamma_{\mathrm{Top},fluct}$	Variogram of the relative fluctuations of the upper boundary of the ML. To exclude a potential linear drift in the fluctuations with the horizontal distance, the variogram was calculated on the *residuals* of a linear regression of fluctuations vs distance.
$\gamma_{\mathrm{Thickness}}$	Variogram of the thickness of the ML. To exclude a potential linear drift in the fluctuations with the horizontal distance, the variogram was calculated on the *residuals* of a linear regression of thickness vs distance.

Table 1: Descriptors of the ML geometry

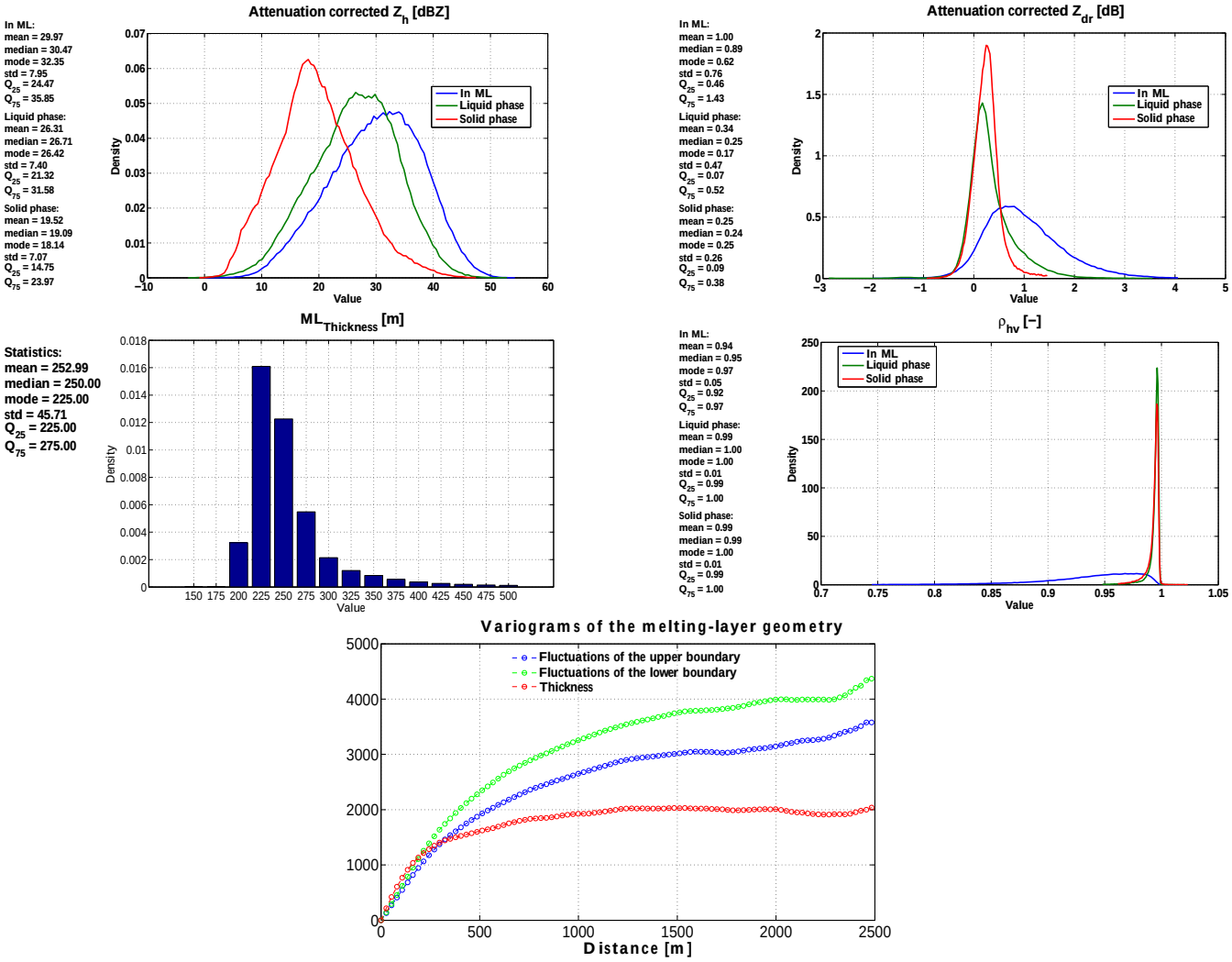

Figure 3: Polarimetric signatures and geometry of the ML observed during the radar campaigns in Ardèche (France) in fall 2012

Concerning the distributions of the different polarimetric variables within the ML and in solid and liquid phases (Figure 3), let us first remark that horizontal reflectivities and differential reflectivites are both high inside the ML, close to respectively 37 dBZ and 1.2 dB. The solid phase is marked by significantly lower values in Z_{dr} and Z_h which is probably due to the smaller size of solid hydrometeors, their smaller dielectric constant and their higher symmetry. Note that this would not be the case in the presence of hail. In the ML, ρ_{hv} shows a strong mode around 0.93 and its distribution is much wider than outside of the ML where, as expected, only high values are present. The fact that low values of ρ_{hv} are only present in the detected ML shows that, on average, the algorithm seems to work reasonably well.

Concerning the geometry of the ML we observe that the distribution of the ML thickness shows a right-skewed distribution: the ML can be much larger than on average but cannot be much thinner. Generally the ML doesn't get much thinner than 200 meters. This minimal height could be related to the thermodynamics of water drops and the lapse rates in the atmosphere. By looking at the variograms of the ML geometry, we can state that the fluctuations of the upper and lower boundary follow the same trends with similar semivariances. Most fluctuations appear at small scale which shows that the structure of the ML is essentially a flat horizontal layer with possibly a linear trend (not visible here due to detrending).

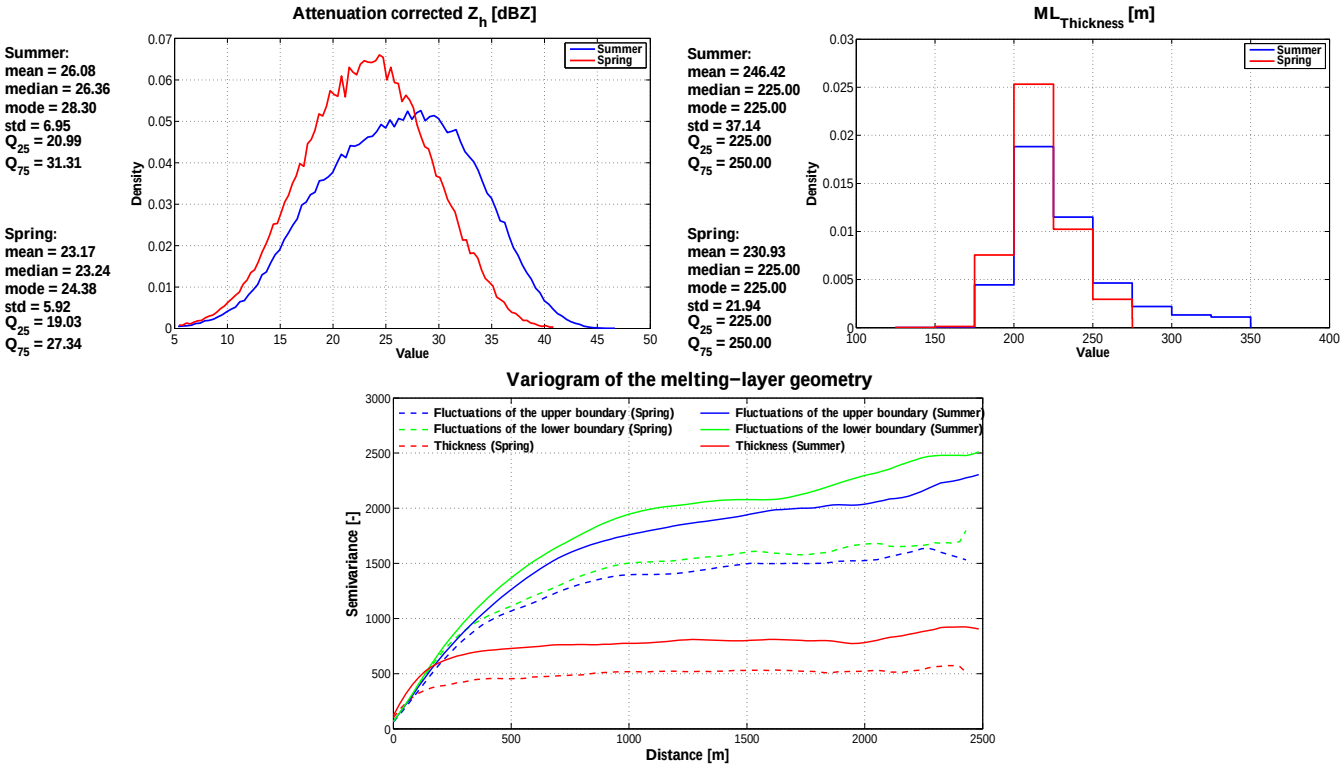

Figure 4: Polarimetric signatures and geometry of the ML observed during the radar campaigns in Davos (Swiss Alps) in spring and summer 2010

For the Davos dataset we compared the characteristics of the ML for the spring and the summer 2010 (Figure 4). It appears that both Z_h as well as the thickness of the ML seem to be larger in summer. The fluctuations of the ML are also slightly larger in summer but with a very similar tendency. It is still unclear why these differences occur and a thorough analysis will be made. It might be possible that a small number of high intensity events occuring in summer bias the distributions. The statistics of the ML seem quite close to the ones in Ardèche with a very similar distribution in thickness and shape of the variograms with however a slightly weaker intensity.

The size of the Great Plains dataset is much smaller (only 72 timesteps) and the validity of a comparison with the other datasets is quite limited. It appears however that the thickness of the ML is higher than in Ardèche and in Davos (Figure 5) but this is probably related to the high average reflectivity.

Additional comparisons within and between the datasets will be made in the future in order to gain more information about the ML variability.

Acknowledgement

We would like to thank Danny Scipion for his help on the ML detection and the projection of radar data, W. Krajewski and the Iowa team for providing IFloods data, Jacopo Grazioli for the processing of raw radar data as well as his help on dual-polarimetry, attenuation-correction and all kind of radar related topics and finally Tim Raupach for all his help with various IT related topics.

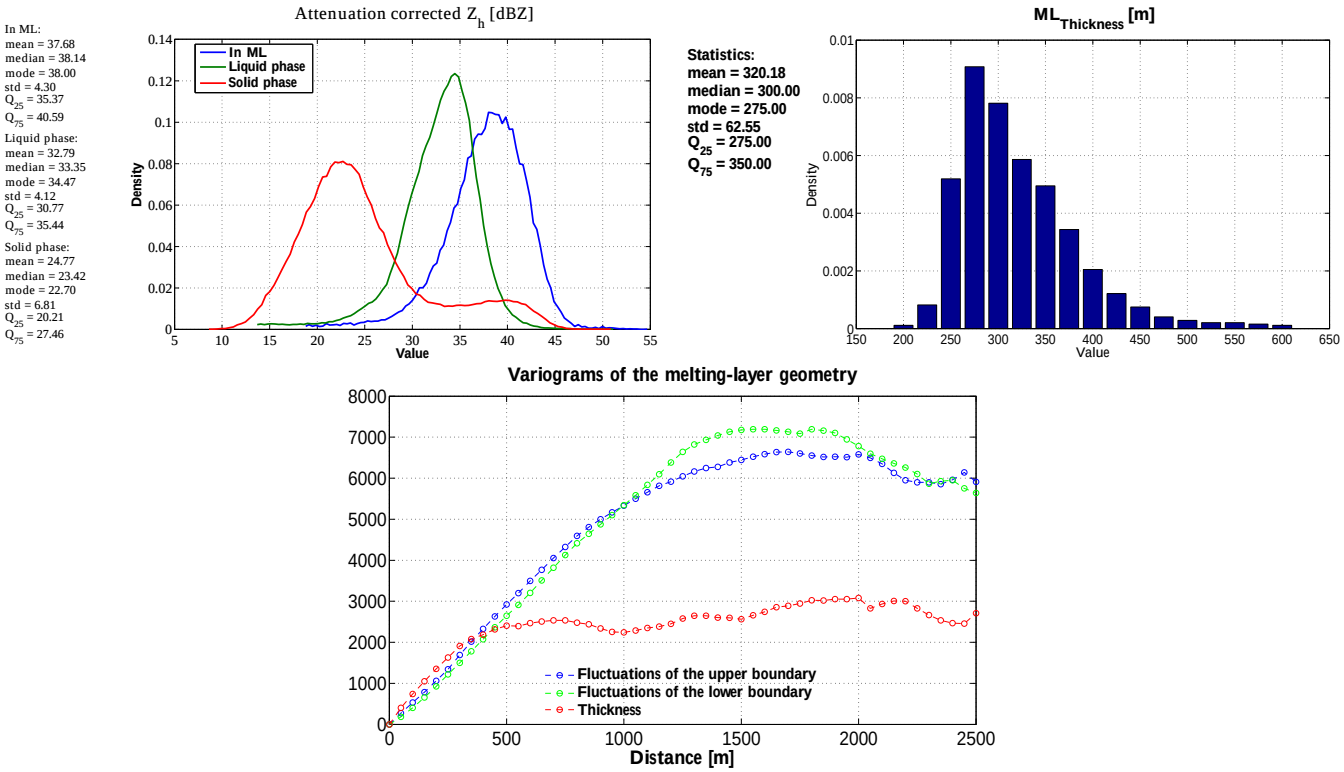

Figure 5: Polarimetric signatures and geometry of the ML observed during the IFLOODS campaign in Iowa (spring 2013).

References

R. Doviak and D. Zrnić, *Doppler radar and weather observations, second edition*. Dover Publications, 2006.

S. E. Giangrande, J. M. Krause, and A. V. Ryzhkov, "Automatic designation of the melting layer with a polarimetric prototype of the wsr-88d radar," *J. Appl. Met. Clim.*, vol. 47, pp. 1354–1364, 2007.

S. Y. Matrosov, K. A. Clark, and D. E. Kingsmill, "A polarimetric radar approach to identify rain, melting-layer, and snow regions for applying corrections to vertical profiles of reflectivity," *J. Appl. Meteorol. Clim.*, vol. 46, no. 2, pp. 154–166, 2007.

J. Testud, E. Le Bouar, E. Obligis, and M. Ali-Mehenni, "The rain profiling algorithm applied to polarimetric weather radar," *J. Atmos. Oceanic Technol.*, vol. 17, no. 3, pp. 332–356, 2000.